Amorphous Solid Model of Vectorial Hopfield Neural Networks

Filippo Gallavotti* and Alessio Zaccone†

Department of Physics "A. Pontremoli", University of Milan, via Celoria 16, 20133 Milan, Italy

We present a vectorial extension of the Hopfield associative memory model inspired by the theory of amorphous solids, where binary neural states are replaced by unit vectors $\mathbf{s}_i \in \mathbb{R}^3$ on the sphere S^2. The generalized Hebbian learning rule creates a block-structured weight matrix through outer products of stored pattern vectors, analogous to the Hessian matrix structure in amorphous solids. We demonstrate that this model exhibits quantifiable structural properties characteristic of disordered materials: energy landscapes with deep minima for stored patterns versus random configurations (energy gaps ~ 7 units), strongly anisotropic correlations encoded in the weight matrix (anisotropy ratios $\sim 10^2$), and order-disorder transitions controlled by the pattern density $\gamma = P/(N \cdot d)$. The enhanced memory capacity ($\gamma_c \approx 0.55$ for a fully-connected network) compared to binary networks ($\gamma_c \approx 0.138$) and the emergence of orientational correlations establish connections between associative memory mechanisms and amorphous solid physics, particularly in systems with continuous orientational degrees of freedom. We also unveil the scaling with the coordination number Z of the memory capacity: $\gamma_c \sim (Z - 6)$ from the isostatic point $Z_c = 6$ of the 3D elastic network, which closely mirrors the scaling of the shear modulus $G \sim (Z - 6)$ in 3D central-force spring networks.

I. INTRODUCTION

The Hopfield model [1] has served as a cornerstone for understanding associative memory in neural networks and artificial intelligence. In its classical formulation, N binary neurons $s_i \in \{-1, +1\}$ evolve according to symmetric interactions W_{ij} defined by the Hebbian rules from stored patterns. The model's dynamics minimizes an energy function $E = -\frac{1}{2}\sum_{ij} W_{ij} s_i s_j$, leading to pattern retrieval through convergence to energy minima.

Recent developments have explored connections between neural network models and the physics of disordered materials, in particular spin glasses [2, 3] but also jammed packings [4, 5] and random resistor and memristive networks [6] and elastic networks [7]. In particular, recent work has been focused on understanding the close relationship between the "cost landscape" and the "physical landscape" as embodied by the cost Hessian matrix and the physical Hessian matrix, respectively [8].

The mathematical structure of neural networks shares fundamental similarities with amorphous solids, particularly in the organization of interaction matrices and the emergence of multiple metastable states. The Hessian matrix in amorphous solids, describing elastic interactions between particles, exhibits random block structure analogous to potential weight matrices in neural networks with vectorial degrees of freedom.

Motivated by this analogy, we introduce a multi-dimensional generalization of the Hopfield model. Each neuron is characterized by a unit vector $\mathbf{s}_i \in \mathbb{R}^3$, and interactions are constructed through outer products following a vectorial Hebbian rule. This approach leverages the concept of random block matrices previously introduced in the context of amorphous solids [9, 10] and only lately adopted in neural network theory [3].

The vectorial extension is not merely a mathematical generalization but reflects physical systems where orientational degrees of freedom play crucial roles, such as in liquid crystals, polymeric glasses, and biological networks (e.g. the cytoskeleton). Our approach reformulates the traditional Hopfield framework in terms of block-structured random matrices, enabling systematic comparison of learning efficiency and computational properties with classical binary models [11]. We shall start by reviewing the basic binary Hopfield model.

II. MODEL DEFINITION

We consider 3D networks of N nodes (neurons) connected by 3D vectors ("bonds" or synapses) as depicted in Fig. 1. In the amorphous solid analogy, the connections between nodes are represented by springs with spring constant κ [12–14].

A. Classical Hopfield Network

The binary Hopfield model consists of N neurons with states $s_i \in \{-1, +1\}$. To store P patterns $\{\boldsymbol{\xi}^\mu\}_{\mu=1}^P$ where $\boldsymbol{\xi}^\mu = (\xi_1^\mu, \ldots, \xi_N^\mu)$ with $\xi_i^\mu \in \{-1, +1\}$, the weight matrix is constructed using the Hebbian rule:

$$W_{ij} = \frac{1}{N} \sum_{\mu=1}^{P} \xi_i^\mu \xi_j^\mu \qquad (1)$$

with $W_{ii} = 0$ (no self-connections) and $W_{ij} = W_{ji}$ (symmetry).

The dynamics follows asynchronous updates: $s_i \leftarrow \text{sign}\left(\sum_j W_{ij} s_j\right)$, which minimizes the energy function $E = -\frac{1}{2}\sum_{ij} W_{ij} s_i s_j$. In words, this means that neuron i looks at the total input it receives from other neurons and updates its state accordingly, such that $\Delta E \leq 0$ is

* filippo.gallavotti@studenti.unimi.it
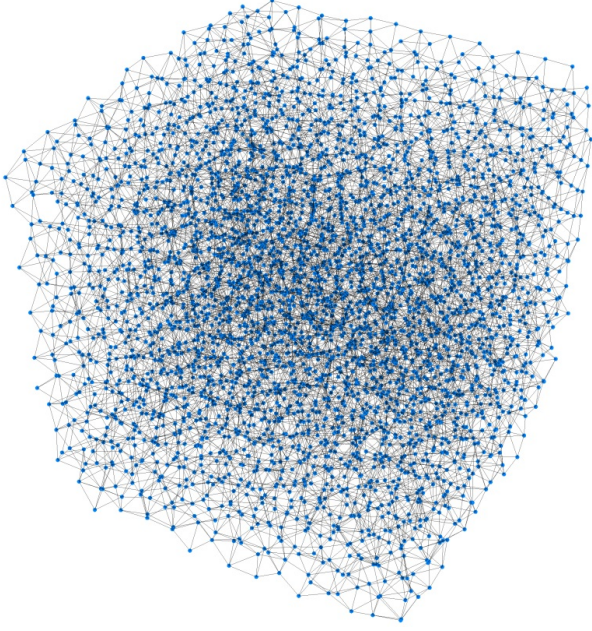† alessio.zaccone@unimi.it

FIG. 1. Rendering of a 3D network of N nodes with an average coordination number $Z = 7$ and a fairly uniform distribution of orientation angles.

guaranteed. Pattern retrieval occurs when the system converges to stored configurations from partial or noisy initial states.

B. Vectorial Extension

In the vectorial model, each neuron i is characterized by a unit vector $\mathbf{s}_i \in \mathbb{R}^3$ with $|\mathbf{s}_i| = 1$. We store P patterns $\{\boldsymbol{\xi}^\mu\}_{\mu=1}^P$, where each pattern consists of N random unit vectors uniformly distributed on S^2:

$$\boldsymbol{\xi}^\mu = (\boldsymbol{\xi}_1^\mu, \ldots, \boldsymbol{\xi}_N^\mu), \quad |\boldsymbol{\xi}_i^\mu| = 1. \tag{2}$$

The weight matrix is constructed through a vectorial Hebbian rule using outer products:

$$\mathbf{W}_{ij} = \frac{1}{N} \sum_{\mu=1}^P \boldsymbol{\xi}_i^\mu \otimes \boldsymbol{\xi}_j^\mu \tag{3}$$

where $\otimes$ denotes the outer product, yielding 3×3 matrices $\mathbf{W}_{ij}$ for each neuron pair ij. The global weight matrix $\mathbf{W}$ has dimensions $3N \times 3N$ with block structure [10].

This construction parallels the Hessian matrix in amorphous solids [9]. For elastic interactions between particles at positions $\mathbf{r}_i$, the Hessian elements are:

$$H_{ij}^{\alpha\beta} = \kappa_{ij} n_{ij}^\alpha n_{ij}^\beta \tag{4}$$

where κ_{ij} is the spring constant and $\mathbf{n}_{ij}$ is the unit vector along the bond direction, defined as:

$$\mathbf{n}_{ij} = (\sin\theta\cos\phi, \sin\theta\sin\phi, \cos\theta), \tag{5}$$

with $\alpha, \beta = \{x, y, z\}$. Again, self-interactions have been ignored. The mathematical structure is identical to Eq. (3), with stored patterns playing the role of sets of bond directions.

The energy function becomes:

$$E(\mathbf{s}) = -\frac{1}{2} \sum_{i,j=1}^N \mathbf{s}_i^T \mathbf{W}_{ij} \mathbf{s}_j \tag{6}$$

The dynamics preserves the unit vector constraint through normalization: each neuron receives a local field $\mathbf{h}_i = \sum_{j \neq i} \mathbf{W}_{ij} \mathbf{s}_j$ and updates according to $\mathbf{s}_i^{\text{new}} = \mathbf{h}_i / |\mathbf{h}_i|$.

III. RESULTS

A. Memory Capacity and Network Connectivity

We investigate the relationship between memory capacity and network topology by examining the coordination number Z, defined as the average number of connections per neuron. Figure 2 demonstrates the critical dependence of memory capacity γ_c on coordination number Z. The capacity increases monotonically from $\gamma_c \approx 0.011$ at $Z = 6.001$ to $\gamma_c \approx 0.255$ for $Z = 9$, in an approximately linear way.

The value $Z = 6$ represents a critical threshold (isostatic point) in three-dimensional central-force elastic networks where mechanical rigidity vanishes (coming from $Z > 6$) due to nonaffine relaxations [9] and in agreement with Maxwell's constraint counting. This connection to rigidity percolation theory provides a physical interpretation of memory capacity limitations in terms of the network mechanical stability. The connection is motivated by the observation, reported here in Fig. 2, that $\gamma_c \sim (Z-6)$, which is the same scaling of the shear modulus, $G \sim (Z-6)$ in central-force 3D elastic networks and in frictionless random sphere packings [9, 15, 16]. We also recall that the isostatic point $Z_c = 6$ coincides with the random close packing (RCP) or maximally-random jammed state in assemblies of hard spheres [17, 18].

B. Orientation Distribution Effects on Memory Performance

We examine how pattern orientation distributions affect memory capacity by generating patterns using randomly distributed orientations for $\mathbf{n}_{ij}$. In particular, because the orientation of each unit vector $\mathbf{n}_{ij}$ is determined by a set of two angles $\{\theta, \phi\}$, cf. Eq. (5), both θ and ϕ are described, separately, by a Gaussian distribution normalized over the respective domains, i.e. $[0, \pi]$ for θ and $[0, 2\pi]$ for ϕ. In the limit of a completely uniform distribution $\sigma \to \infty$, the probability of a certain orientation in the solid angle is identically equal to $1/4\pi$ [9, 19].
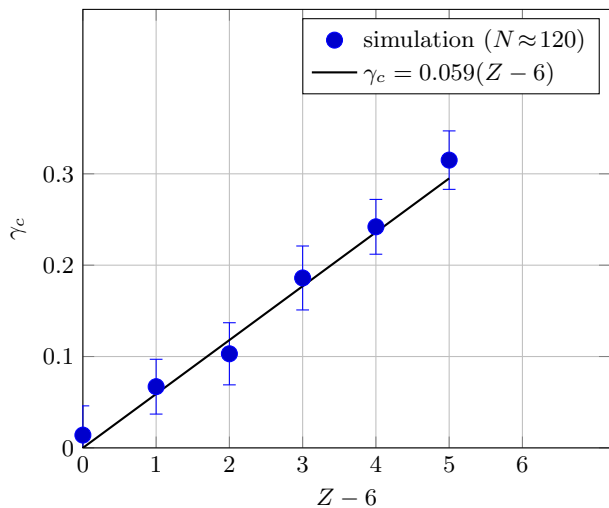
FIG. 2. Critical storage load $\gamma_c = P_c/(Nd)$ of the 3-D Hopfield network with $N = 120$ neurons and $d = 3$ as a function of the coordination number Z. For each Z, the critical pattern number P_c is determined via an 11-step bisection (collapse threshold 0.02, retrieval threshold 0.65), using a single fixed symmetric adjacency, 2 pattern reservoirs per bisection step, and 150 random initial-state trials. Each point is the mean over 6 independent replicas; error bars give the corresponding standard deviations. The results display the mean-field scaling of γ_c with $(Z - 6)$.

Figure 3 reveals a sharp transition in memory capacity as a function of the bond-orientation diversity. Indeed, a sharp drop in the memory capacity occurs upon approaching $\sigma \approx 1$ from lower values. This observation suggests that a certain (modest) degree of bond-orientational order is beneficial to optizime the memory capacity in the otherwise random networks.

For sufficiently narrow distributions ($\sigma < 1$), the capacity remains near unity, indicating that patterns with similar orientations are easily distinguishable. After the dramatic capacity drop at $\sigma \approx 1$, where γ_c drops to approximately 0.1, the memory capacity for large $\sigma > 2$ then approaches the uniform distribution limit of sparse networks, $\gamma_c \approx 0.05$, asymptotically. A partial recover may occur around $\sigma \approx 2$, which, however, does not exceed $\gamma_c \approx 0.1$.

This behavior reflects competing effects of orientational order and statistical independence. Narrower distributions create stronger orientational correlations that facilitate retrieval, while uniform distributions provide geometric separation despite reduced correlations.

C. Energy Landscape Structure

The vectorial Hopfield model creates energy landscapes with multiple local minima corresponding to stored patterns. We quantify the energy separation between stored configurations and random states to characterize pattern
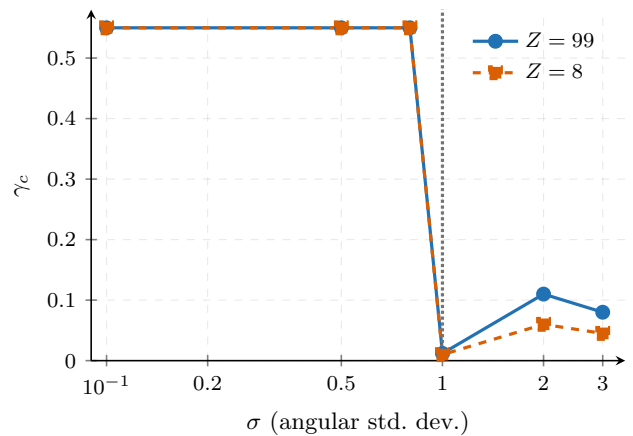

FIG. 3. Characteristic behaviour of the critical storage load (memory capacity) $\gamma_c = P_c/(Nd)$ as a function of the angular standard deviation σ of the pattern-orientation distribution for two network connectivities Z. The blue curve refers to a nearly fully–connected network ($N = 80$, $Z = 99 \simeq N - 1$), while the orange curve corresponds to the same system with a much lower coordination number ($Z = 8$). For sufficiently narrow distributions ($\sigma \lesssim 1$) both networks reach the ceiling imposed by the reservoir size ($P_{\max} = 0.50\,Nd \Rightarrow \gamma_c = 0.55$). A sharp drop occurs at $\sigma \simeq 1$, signaling the onset of pattern interference. In the uniform limit ($\sigma \gtrsim 2$) the dense network recovers a capacity of $\gamma_c \approx 0.08$, whereas the sparse network settles at $\gamma_c \approx 0.05$, consistent with the expected scaling $\gamma_c \propto Z/(N - 1)$. Each point is the average of two independent replicas obtained via a nine-step bisection procedure (collapse threshold $q < 0.02$, retrieval threshold 0.65) with 60 random trials per step; error bars are omitted as they are smaller than the marker size.

stability.

For system parameters $N = 25$ and $\gamma = 0.1$, stored patterns exhibit mean energies approximately 7 units lower than random configurations. This substantial energy gap ensures robust pattern retrieval against initialization noise. The energy function:

$$E(\mathbf{s}) = -\frac{1}{2} \sum_{i,j=1}^{N} \mathbf{s}_i^T \mathbf{W}_{ij} \mathbf{s}_j \qquad (7)$$

naturally creates this hierarchical structure through the outer product construction of the weight matrix.

The energy gap magnitude scales inversely with pattern density, decreasing as γ approaches the critical threshold where memory capacity is lost. This behavior parallels metastable state hierarchies observed in glass-forming systems [20–22].

D. Spectral Properties and Weight Matrix Structure

The eigenvalue spectrum of the weight matrix, presented in Fig. 4, provides information on computational

properties at different pattern densities. With reference to Fig. 4, we observe distinct spectral regimes, as follows.

For low pattern density ($\gamma = 0.05$), the spectrum is dominated by isolated eigenvalues corresponding to stored patterns, with the bulk distribution concentrated near zero. At intermediate pattern density ($\gamma = 0.1 - 0.2$), a spectral bulk emerges with pattern eigenvalues appearing as outliers. For high density ($\gamma = 0.5$), the spectrum transitions towards a random matrix behavior.

The spectral density evolution with γ reflects the crossover from a memory-dominated regime to a noise-dominated regime. The critical pattern density γ_c corresponds to the point where pattern eigenvalues merge with the spectral bulk, marking the loss of pattern discriminability.

E. Basin of Attraction Analysis

The dynamics exhibits convergence behavior that depends critically on initialization and pattern density. We characterize basin properties through convergence statistics, as follows.

The convergence time scales logarithmically with the system size N for successful retrievals. The basin size decreases as γ approaches γ_c, following approximately exponential scaling. Near the memory capacity threshold, basins develop complex boundaries leading to sensitive dependence on initial conditions.

The unit vector normalization constraint creates dynamics on the product manifold $S^2 \times S^2 \times \cdots \times S^2$. This geometric constraint preserves pattern structure but introduces complexity compared to unconstrained dynamics. The update rule:

$$\mathbf{s}_i^{(t+1)} = \frac{\mathbf{h}_i^{(t)}}{|\mathbf{h}_i^{(t)}|}, \quad \mathbf{h}_i^{(t)} = \sum_{j \neq i} \mathbf{W}_{ij} \mathbf{s}_j^{(t)} \tag{8}$$

ensures convergence to fixed points while maintaining the spherical constraint.

F. Correlation Structure in the Weight Matrix

The block-structured weight matrix $\mathbf{W}$ encodes orientational correlations through its 3×3 blocks $\mathbf{W}_{ij}$. We analyze correlation properties by examining (i) the Frobenius norm $|\mathbf{W}_{ij}|_F$, measuring interaction intensity, and (ii) the anisotropy ratio $\lambda_{\max}/\lambda_{\min}$ of $\mathbf{W}_{ij}^T \mathbf{W}_{ij}$, measuring directional bias.

For typical systems, we observe mean correlation strength $\langle |\mathbf{W}_{ij}|_F \rangle \approx 0.02$ and mean anisotropy ratio $\langle \lambda_{\max}/\lambda_{\min} \rangle \approx 15$. The high anisotropy ratios indicate strongly directional interactions, reflecting the vectorial nature of stored patterns.

This correlation structure creates emergent organization in the weight matrix, with enhanced correlations between blocks corresponding to pattern pairs with similar orientations.

IV. DISCUSSION AND CONCLUSIONS

The vectorial Hopfield model inspired by amorphous solids demonstrates enhanced memory capacity compared to binary networks, with maximum critical capacity $\gamma_c \approx 0.55$ for fully-connected non-orientationally uniform random elastic networks. This improvement over the standard binary Hopfield model (which has $\gamma_c \approx 0.138$) stems from the increased dimensionality and from the geometric structure of the pattern space. Non-uniform distributions of bond-orientations (standard deviation $\sigma < 1$), are realistic for amorphous materials with excluded-volume such as structural glasses or jammed packings [14, 23, 24]. A sharp drop in the memory capacity is observed upon increasing the standard deviation σ of the Gaussian-distributed bond-orientation probability, at $\sigma \approx 1$.

The analysis of the memory capacity γ_c as a function of the 3D network coordination number Z reveals a capacity scaling $\gamma_c \sim (Z - 6)$ for $Z > 6$. This observation establishes an important connection with rigidity percolation theory and nonaffine deformation theory of amorphous solids, where the shear modulus G of frictionless jammed packings and of central-force elastic networks exhibits exactly the same scaling, $G \sim (Z - 6)$, with respect to the isostatic point $Z_c = 6$ [9, 16].

The energy landscape analysis confirms robust pattern storage through substantial energy gaps between stored patterns and random configurations. Spectral analysis as shown in the plots of the eigenvalue distributions of the weight matrix, reveals transitions between memory-dominated and noise-dominated regimes, providing insight into the capacity limitations.

These results establish the 3D vectorial Hopfield model as a potentially powerful framework for understanding associative memory in continuous variable systems, with applications to pattern recognition tasks involving orientational or directional information.

The enhanced capacity and altered dynamical properties of vectorial Hopfield networks have implications for artificial neural network design. The three-dimensional embedding provides natural advantages for pattern separation and storage (e.g. through deeper energy minima), suggesting that vectorial architectures might offer computational benefits in specific applications.

The requirement for appropriate initialization strategies in vectorial networks parallels challenges in training modern deep networks, where initialization schemes critically affect convergence. The insights from vectorial Hopfield dynamics may inform initialization strategies for more complex vectorial architectures.

The block-structured weight matrices arising from vectorial Hebbian learning create natural hierarchical organizations that, in future work, could be exploited
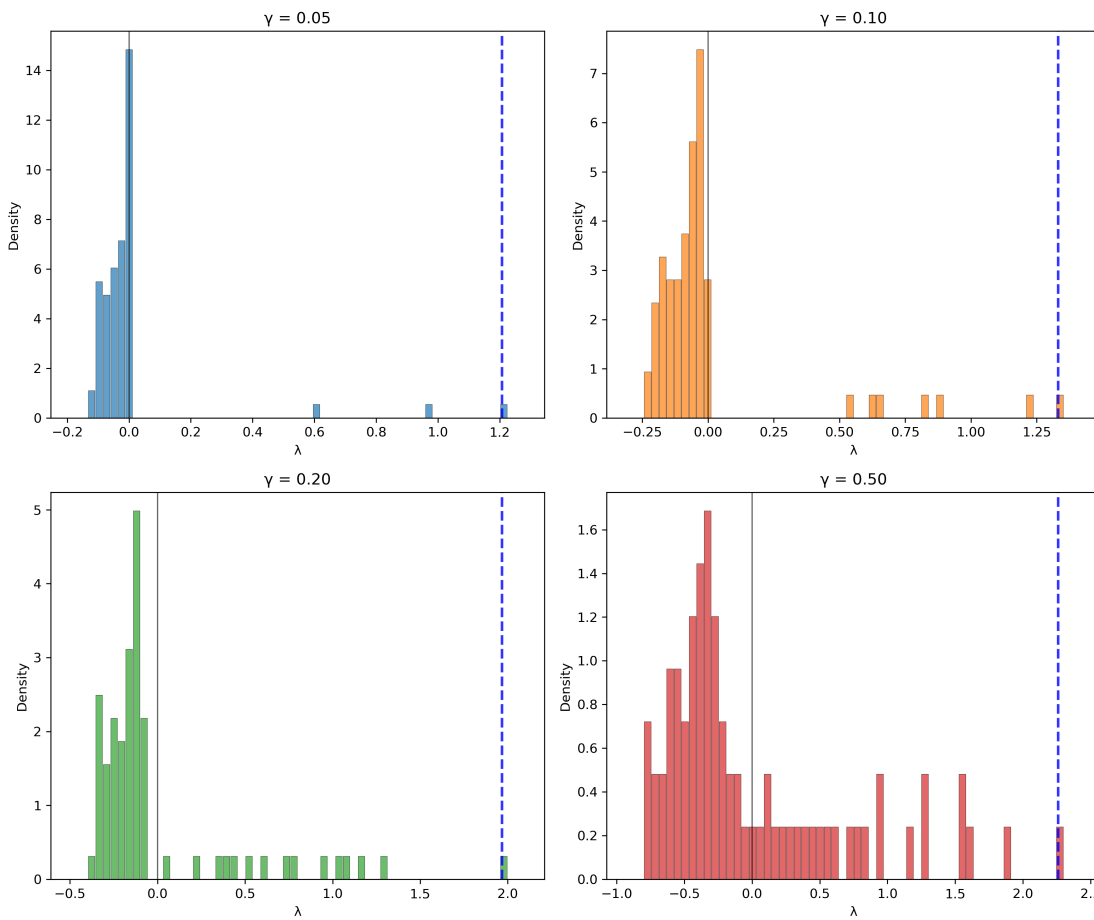
FIG. 4. Evolution of spectral density $\rho(\lambda)$ with different pattern capacities $\gamma = P/(Nd)$. Low density shows concentrated bulk near zero with isolated positive eigenvalues, while high density exhibits broad continuous distributions, indicating pattern interference onset.

in network architectures designed for specific pattern recognition tasks involving continuous variables or orientational data. A natural extension of the proposed model is in the direction of dense associative memory models, e.g. by extending the standard linear Hebbian rule with the use of nonlinear higher-order functions like $F(x) = x^n/n$ (Krotov-Hopfield) [25].

APPENDIX

In Fig. 5 we show the typical time evolution of the Lyapunov energy as a function of the number of updated steps, giving evidence of the monotonic convergence of the dynamics in the proposed neural network model.

[1] J. J. Hopfield, Proceedings of the National Academy of Sciences **79**, 2554 (1982), https://www.pnas.org/doi/pdf/10.1073/pnas.79.8.2554.

[2] D. J. Amit, H. Gutfreund, and H. Sompolinsky, Phys. Rev. A **32**, 1007 (1985).

[3] F. Nicoletti, F. D'Amico, and M. Negri, "Statistical mechanics of vector hopfield network near and above satu-
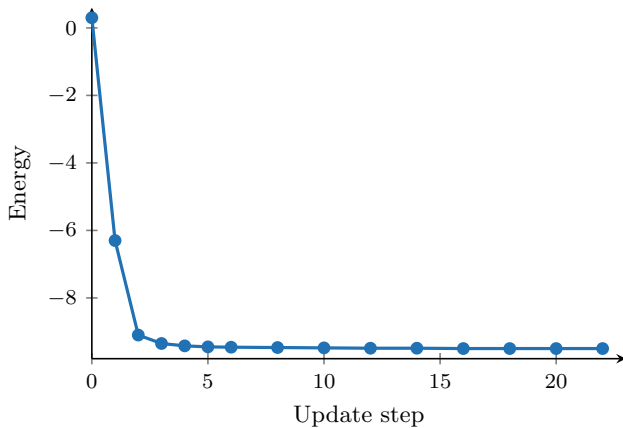
FIG. 5. Time evolution of the Lyapunov energy $E(t) = -\frac{1}{2} \mathbf{s}^\top W \mathbf{s}$ for a single synchronous run of the vector–Hopfield model with $N = 25$ neurons, $d = 3$, and $P = 5$ stored patterns. After a rapid decay in the first three updates the energy settles on the minimum corresponding to the retrieved pattern, confirming the monotonic convergence of the dynamics.

ration," (2025), arXiv:2507.02586 [cond-mat.dis-nn].

[4] M. Geiger, S. Spigler, S. d'Ascoli, L. Sagun, M. Baity-Jesi, G. Biroli, and M. Wyart, Phys. Rev. E **100**, 012115 (2019).

[5] G. Zhang, D. J. Heeger, and S. Martiniani, "Contrastive self-supervised learning as neural manifold packing," (2025), arXiv:2506.13717 [cs.LG].

[6] S. G. Hu, Y. Liu, Z. Liu, T. P. Chen, J. J. Wang, Q. Yu, L. J. Deng, Y. Yin, and S. Hosaka, Nature Communications **6**, 7522 (2015).

[7] L. E. Altman, M. Stern, A. J. Liu, and D. J. Durian, Phys. Rev. Appl. **22**, 024053 (2024).

[8] M. Stern, M. Guzman, F. Martins, A. J. Liu, and V. Balasubramanian, Phys. Rev. Lett. **134**, 147402 (2025).

[9] A. Zaccone and E. Scossa-Romano, Physical Review B **83**, 184205 (2011).

[10] G. M. Cicuta, J. Krausser, R. Milkus, and A. Zaccone, Phys. Rev. E **97**, 032113 (2018).

[11] J. A. Hertz, A. S. Krogh, and R. G. Palmer, *Introduction to the Theory of Neural Computation*, Santa Fe Institute Studies in the Sciences of Complexity, Vol. 1 (Addison–Wesley, Reading, MA, 1991) p. 327.

[12] R. Milkus and A. Zaccone, Phys. Rev. B **93**, 094204 (2016).

[13] R. Milkus and A. Zaccone, Phys. Rev. E **95**, 023001 (2017).

[14] A. Zaccone, *Theory of Disordered Solids* (Springer, Cham, 2023).

[15] C. S. O'hern, L. E. Silbert, A. J. Liu, and S. R. Nagel, Physical Review E **68**, 011306 (2003).

[16] A. Zaccone, Journal of Applied Physics **137**, 050901 (2025), https://pubs.aip.org/aip/jap/article-pdf/doi/10.1063/5.0245684/20382996/050901_1_5.0245684.pdf.

[17] S. Torquato and F. H. Stillinger, Reviews of modern physics **82**, 2633 (2010).

[18] A. Zaccone, Physical Review Letters **128**, 028002 (2022).

[19] A. Zaccone, J. R. Blundell, and E. M. Terentjev, Phys. Rev. B **84**, 174119 (2011).

[20] G. Biroli and J. Kurchan, Phys. Rev. E **64**, 016101 (2001).

[21] D. Han, D. Wei, J. Yang, H.-L. Li, M.-Q. Jiang, Y.-J. Wang, L.-H. Dai, and A. Zaccone, Phys. Rev. B **101**, 014113 (2020).

[22] P. Charbonneau, J. Kurchan, G. Parisi, P. Urbani, and F. Zamponi, Nature Communications **5**, 3725 (2014).

[23] A. Zaccone and E. M. Terentjev, Journal of Applied Physics **115**, 033510 (2014), https://pubs.aip.org/aip/jap/article-pdf/doi/10.1063/1.4862403/15126547/033510_1_online.pdf.

[24] M. Schlegel, J. Brujic, E. M. Terentjev, and A. Zaccone, Scientific Reports **6**, 18724 (2016).

[25] D. Krotov and J. Hopfield, "Large associative memory problem in neurobiology and machine learning," (2021), arXiv:2008.06996 [q-bio.NC].